PERGAMON

International Journal of Heat and Mass Transfer 44 (2001) 1849–1856

International Journal of HEAT and MASS TRANSFER

www.elsevier.com/locate/ijhmt

A molecular dynamics study on surface tension of microbubbles

S.H. Park [a], J.G. Weng [b], C.L. Tien [b,*]

[a] *Department of Mechanical Engineering, Hongik University, Seoul 121-791, South Korea*
[b] *Department of Mechanical Engineering, University of California, Berkeley, CA 94720, USA*

Received 31 May 2000; received in revised form 18 July 2000

Abstract

This work is the first molecular dynamics (MD) study on the surface tension of bubbles and their related characteristics. Compared to thin films or droplets, bubbles have not been investigated using the MD simulation method for their properties owing to their inherent difficulties. To confirm their existences, a stable bubble regime with respect to simulation domain sizes is defined for the Lennard–Jones molecules. As well as the local densities, normal and tangential pressure components are calculated and used for the estimation of bubble surface tensions. While the surface tension of droplets varies as predicted by Tolman's equation, that of bubbles changes slightly and is greater than the value for the planar interface by 15% or less. In addition, effects of solute molecules on the surface tension of bubbles in a binary molecule system are investigated for the cases of less and more attractive interactions between solute and solvent molecules.

1. Introduction

The main objective of this work is to give a systematic estimation of bubble surface tension and related characteristics using the molecular dynamics (MD) simulation method. In this simulation a bubble center is defined as the mass center of void space. By centering the bubble in the calculation domain, distributions of density and pressure tensor components are obtained through an averaging process during the production period. Based on the mechanical arguments for the force and moment balances and the mechanical stability [1,2] called as 'mechanical route', bubble surface tensions are calculated together with the corresponding radii.

Interfacial phenomena involved in bubbles, thin films and droplets have attracted the attention of researchers for quite a long time due to their wide applications as well as due to their statistical uncertainties in engineering and science fields [2–4]. Since detailed molecular movements and interactions are critical to estimate the characteristics of the interface, the MD simulation method is frequently applied to produce pseudoexperimental data [5,6]. While a significant number of MD simulations have been conducted on the characteristics of droplets and liquid thin films, much less attention has been paid to the microscopic investigation of bubbles and their characteristics [7] due to their relative difficulties of dealing with higher number densities, estimating the bubble center location, and exploring the uncertainties of the metastable liquid-phase surrounding them. Moreover, recent experimental studies report that a bubble nucleation from microstructures is 'uniquely different from macroscale boiling' [8], which demands a detailed investigation of microscale bubble nucleation phenomena. A bubble, therefore, formed in a microsystem or smaller than that in the macroscale boiling phenomena can be called as a microbubble, which is relevant to be explored by the MD simulation method.

To date, the MD research results available in literature for bubble characteristics are limited to the understanding of the incipient stage of cavitation using a radial distribution function [9], the demonstration of the cavitation in negative pressure by expanding a Lennard–Jones liquid [10,11], and the simulation of the cavitation based on Berthelot tube method and the preliminary characterization of microbubbles [12].

* Corresponding author.

0017-9310/01/$ - see front matter
PII: S0017-9310(00)00244-1

Nomenclature

k_B	Boltzmann's constant
L	simulation domain size
m	mass of molecules
N	number of molecules
P	pressure
r	distance between two molecules or radial coordinate
R	radius
t	time
T	temperature
x, y, z	rectangular coordinates

Greek symbols

α	attraction coefficient
δ	Tolman's length
ε	scale of energy for potential functions
Φ	potential function
γ	surface tension
ρ	number density
σ	scale of length for potential functions

Superscript

*	dimensionless quantity

Subscripts

avg	global average
e	equimolar dividing surface
g	vapor-phase
K	kinetic component
l	liquid-phase
S	surface of tension
N, T	normal and transverse components
U	configurational component
∞	planar interface

This paper conducts a series of canonical ensemble MD simulations to generate a regime map for conditions of stable bubbles as a function of calculation domain sizes. Within the stable bubble regime the density profiles and the normal and transverse components of the pressure tensor are calculated to estimate the surface tension of a bubble following the mechanical route. Using the surface tension of a planar interface as a reference value the surface tensions of bubbles and droplets are compared with the theoretical estimation from the Tolman equation [1,2,13]. In addition, a simple binary molecule system is investigated to understand the effects of foreign molecules on the surface tension of a bubble.

2. Simulation models

In the classical theory the effect of curvature on the surface tension of a small droplet is given by the Tolman equation [1,2,13]

$$\frac{\gamma_S}{\gamma_\infty} = 1 - \frac{2\delta}{R_S} + \cdots, \tag{1}$$

where γ_S and γ_∞ are the surface tensions for a droplet and a planar liquid–vapor interface, respectively and

$$\delta = R_e - R_S, \tag{2}$$

where R_e and R_S are the radii for the equimolar surface and the surface of tension which will be defined later. There is, however, neither a theoretical model to observe the bubble characteristics effectively nor any attempt to investigate the curvature effect of small bubbles from MD approach or experiments. In the current study the MD simulation will be employed because it is a promising tool for the microscopic estimation of the surface tension of a microbubble and for the efficient investigation of related bubble nucleation phenomena and their characteristics.

The intermolecular interactions in this MD study are described by the well-known Lennard–Jones (LJ) 12-6 potential,

$$\Phi(r_{ij}) = 4\varepsilon\left[\left(\frac{\sigma}{r_{ij}}\right)^{12} - \left(\frac{\sigma}{r_{ij}}\right)^{6}\right], \tag{3}$$

where r_{ij} is the distance between two molecules, i and j, and ε and σ are the representative scales of energy and length, respectively. Molecules are placed in a cube of volume L^3 with periodic boundaries in all three dimensions. They move according to the imposed intermolecular forces based on the potential function, Eq. (3), and these movements can be described by the classical momentum equations. The momentum equations are discretized by the "velocity Verlet" algorithm [14]. In the simulation, the total number of molecules N, the total volume L^3, and the average temperature T are kept constant by the momentum scaling method.

To speed up the otherwise time-consuming simulation and to define an initial condition, a slightly subcooled liquid-phase has been prepared and the molecules are selected randomly from the liquid-phase according to the average density in each simulation. A relatively long equilibration period of more than 200,000 time steps, however, is taken to ensure that the system is at the preset condition, since phase-change phenomena usually occur in a metastable situation and thus any small perturbation can incur a remarkable change of the state even after a very long time. This period is followed by a production period of at least 60,000 time steps. During the production period, instantaneous values of

the local density and the local normal pressure component are obtained by dividing the simulation cell into concentric shells of thickness 0.1σ. The densities and the normal pressure components in each shell are accumulated and averaged over the production period.

3. Results and discussion

In this MD study, the cut-off radius r_c beyond which the pair interaction is neglected is set at 3σ without a long-range force correction. The time step is $\Delta t = 5$ fs. All quantities indicated by an asterisk are non-dimensionalized according to σ, ε, and m, which use the values of argon such that $\sigma = 0.34$ nm, $\varepsilon = 1.67 \times 10^{-21}$ J, and $m = 6.63 \times 10^{-26}$ kg. For example, the reduced temperature, length, number density, pressure, and surface tension are $T^* = k_B T/\varepsilon$, $r^* = r/\sigma$, $\rho^* = \rho\sigma^3$, $P^* = P\sigma^3/\varepsilon$, and $\gamma^* = \gamma\sigma^2/\varepsilon$, respectively.

In order to investigate the bubble nucleation process and its characteristics, a grid of void packets is constructed and each void grid is defined as a cubic void cell of side length 0.3σ, in which there are no molecules within 1.2σ from the void cell center, while a relatively larger grid size 0.588σ has been used to visualize the void packet in a heterogeneous nucleation [15]. Since the number of void cells for a stable bubble is greater than 1000 in this study, the void grid size has a minor importance. Its variation between 0.3σ and 0.6σ results in a very little difference unless the number of void cells becomes much smaller than 200, which turns out to be the case of an unstable bubble formation.

On the mass center of void packets the calculation domain is centered artificially, which is critical to obtain relevant average shapes of bubbles and their characteristics. A typical cross-sectional snapshot (15% clipping of the calculation domain around the plane of $y = 0$) of the molecular distribution is shown in Fig. 1. Here, the calculation conditions are $\rho^*_{avg} = 0.6575$, $T^* = 0.818$, and $L^* = 15$. It is noted that the central region can be regarded as a vapor-phase and the outer region of higher density as a liquid-phase. Contrary to the general notion of spherical bubble, the liquid–vapor interface in this microscopic system cannot be defined sharply since the bubble is not perfectly spherical and each phase is not uniform at any given instant during the simulation, necessitating the time averaging procedure.

Local density profiles are calculated by counting and time-averaging the number of molecules in shells of thickness 0.1σ. At $T^* = 0.818$ the density profiles of a single-component molecule system contained in a cubical domain of $L^* = 15$ are shown in Fig. 2 for various average densities (ρ^*_{avg}) smaller than the saturated liquid density of argon, $\rho^*_{l,sat} = 0.776$ [16]. Here, the average density $\rho^*_{avg} = N/L^{*3}$ remains unchanged for each simulation. It is usually understood that the state of density

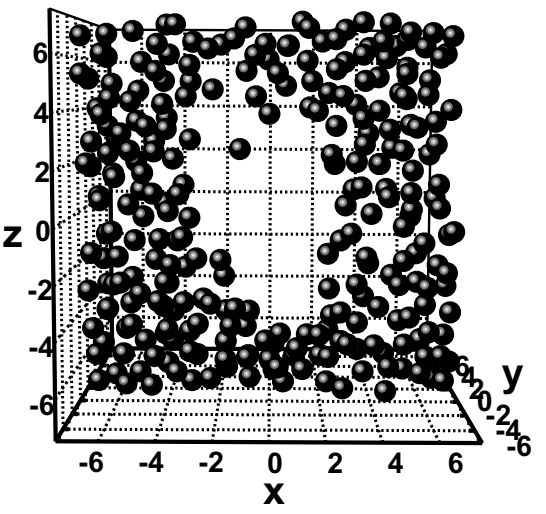

Fig. 1. A cross-sectional snapshot of the molecular distribution of a bubble for $\rho^*_{avg} = 0.6575$, $L^* = 15$, and $T^* = 0.818$.

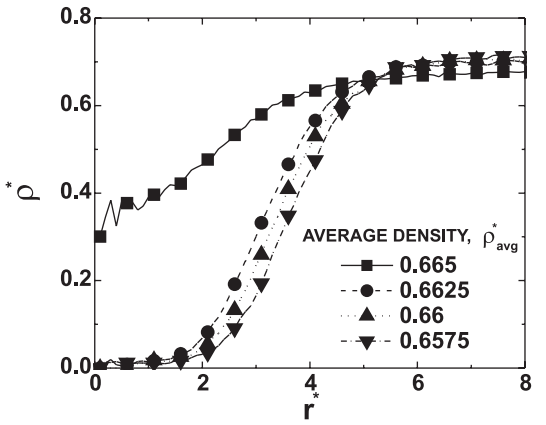

Fig. 2. Local density profiles for various average densities at $L^* = 15$ and $T^* = 0.818$.

lower than that of the saturated liquid state is metastable and may turn into a two-phase equilibrium by a small perturbation. For average densities greater than 0.665, however, which is still much lower than that of the saturated state, it is almost impossible to achieve a stable bubble. Stable bubbles can be observed only for average densities lower than 0.6625. For the case of $\rho^*_{avg} = 0.665$, the local density in the center region is slightly lower than that in the outer region, which implies that some of the unstable bubble embryos form and collapse intermittently, since their lifetimes are too short to be stable. For stable bubbles the vapor density is about 0.01, which is close to that of the experimental value, $\rho^*_{g,sat} = 0.00925$ [16], while the liquid-phase density is about 0.7, which is slightly lower than that of the

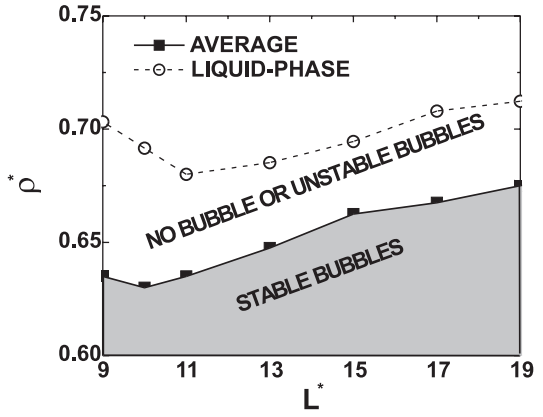

Fig. 3. Regime map for stable bubbles and corresponding liquid-phase densities.

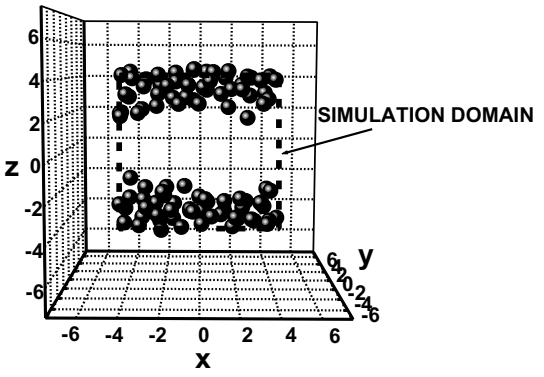

Fig. 4. A cross-sectional snapshot of the molecular distribution of a bubble for $\rho^*_{avg} = 0.635$, $L^* = 9$, and $T^* = 0.818$.

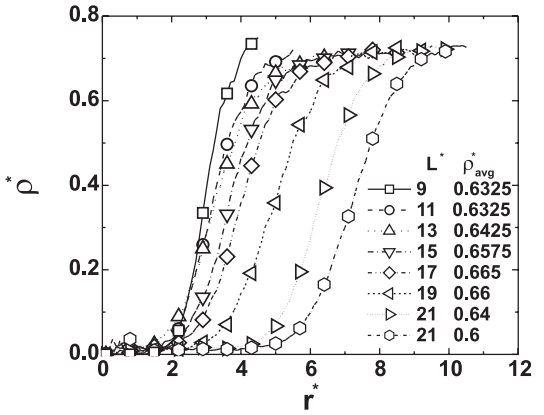

Fig. 5. Local density profiles for various calculation domain sizes and average densities.

saturated liquid-phase. From this it can be understood that the liquid-phase is stretched and thus still in a metastable state.

As represented in Fig. 2, for a fixed calculation domain the average density should be smaller than a critical value to maintain a stable bubble. Fig. 3 defines the calculation domain for the stable bubble nucleation. This figure shows that the critical average density for a bubble formation and the corresponding liquid-phase density decrease with the decrease of the domain size down to $L^* = 11$. In other words, a larger domain is more vulnerable to break-up and more liable to induce a bubble than a smaller domain. This can be understood by the Weibull equation [17], which implies that the probability of failure (nucleation, here) increases exponentially with the specimen volume, from which the size effect of the calculation domain can be understood. In contrast, for domains $L^* < 11$ the average and the liquid-phase densities increase, as the domain size decreases. This might be due to the fact that the liquid-phase region between adjacent bubbles becomes too thin to hold the bubble inside, the liquid-phase region breaks up and thus the adjacent bubbles tend to merge together, as depicted by Fig. 4 (20% clipping around the plane of $y = 0$), whose simulation conditions are $\rho^*_{avg} = 0.635$ and $L^* = 9$. Therefore, the results obtained for domains $L^* < 11$ are significantly interfered by the adjacent domains due to the periodic boundary condition and are questionable.

In Fig. 5 local density profiles of bubbles are shown for various calculation domain sizes and average densities. For the cases of $L^* \geqslant 13$ the density gradients at the edge of the calculation domains are almost zero, while those gradients for $L^* \leqslant 11$ are quite different from zero. For larger calculation domain sizes the interfacial density approaches its liquid-phase density as r^* increases, because the liquid-phase region between the adjacent bubbles is relatively thick enough to maintain spherical uniformity. For smaller domain sizes, however, local densities in the corner region of the domain are quite different from those near the sides or faces of the cubic domain and furthermore, the bubble shape is no longer spherical, as observed in Fig. 4.

Fig. 6 describes the pressure variation, specifically the normal component in the interfacial region from vapor- to liquid-phases as r^* increases. The normal component of the pressure tensor in the spherically symmetric system is

$$P^*_N(r^*) = P^*_K(r^*) + P^*_U(r^*), \tag{4}$$

where the kinetic and the configurational terms [1] are:

$$P^*_K(r^*) = \rho^*(r^*)T^*, \tag{5}$$

$$P^*_U(r^*) = -(4\pi r^*)^{-1} \sum_k \left| \vec{r}^* \cdot \vec{r}^*_{ij} \right| \frac{1}{r^*_{ij}} \frac{d\Phi^*(r^*_{ij})}{dr^*_{ij}}. \tag{6}$$

Similarly to the density profiles shown in Fig. 5, the gradients of the pressure profiles in the edge region of

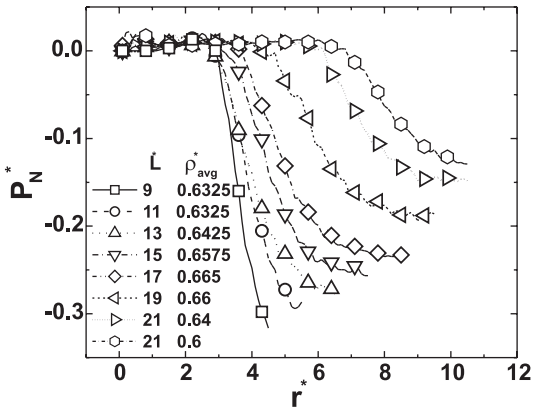

Fig. 6. Local normal pressure profiles for various calculation domain sizes and average densities.

calculation domains $L^* \leqslant 11$ are quite different from zero, since the spherically non-uniform distribution of the density induces the non-uniform pressure distribution. The liquid-phase density in the edge region of each curve increases very slightly with the increase of bubble radius as shown in Fig. 5. The pressure in that region, however, increases considerably, which can be explained by the Laplace equation,

$$\Delta P = \frac{2\gamma_S}{R_S}, \tag{7}$$

where ΔP is the pressure difference between vapor- and liquid-phases.

Although the main concern in this study is the surface tension of a bubble, it is interesting to compare the density and pressure profiles of a bubble, a thin film and a droplet, which are shown in Figs. 7(a)–(c). The density ρ^* and the normal pressure component P_N^* in Figs. 7(a) and (c) are fitted by the *tanh* function, which has been frequently applied to fit the density distribution for a droplet. Data points denoted by symbols are obtained from the MD simulation and lines are from the fitting function, for example,

$$\rho^*(r^*) = \frac{1}{2}\left(\rho_l^* + \rho_g^*\right) - \frac{1}{2}\left(\rho_l^* - \rho_g^*\right)\tanh\left[2(r^* - R_0^*)/D^*\right]. \tag{8}$$

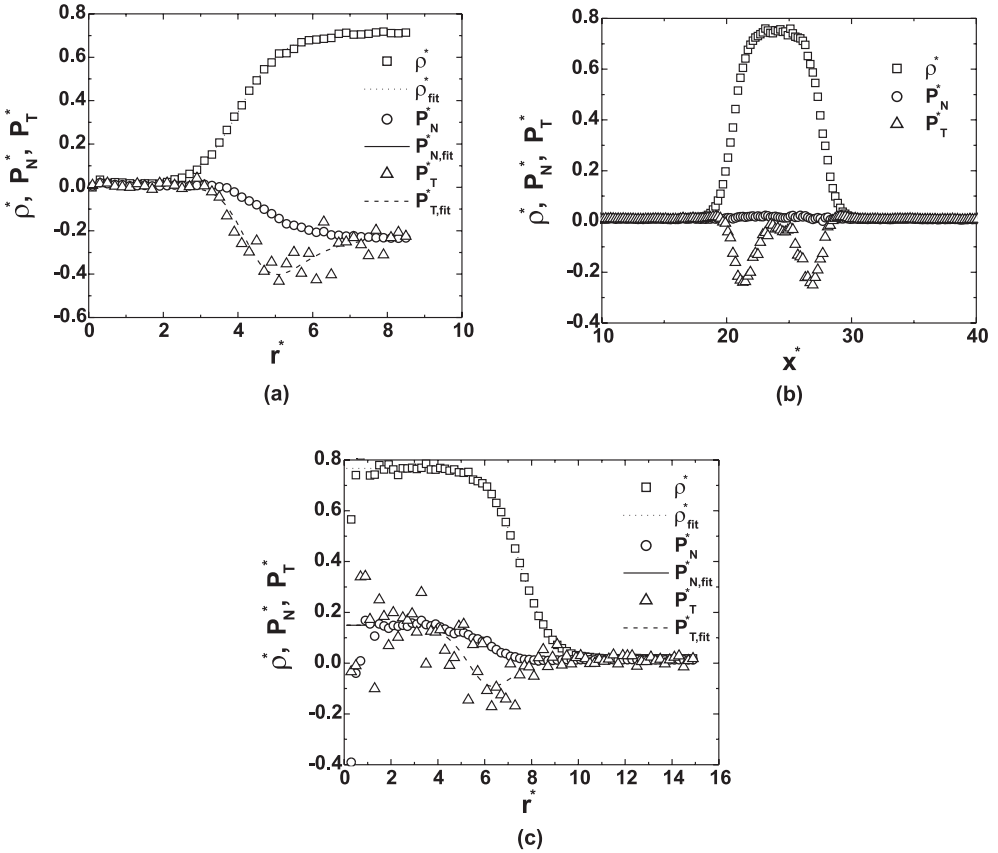

Fig. 7. Profiles of density and pressure tensors: (a) for a bubble at $L^* = 17$; (b) for a thin film at $L^* = 48$; (c) for a droplet at $L^* = 30$.

The transverse pressure component P_T^* can be obtained from mechanical stability under the spherically symmetric assumption and given as

$$P_T^*(r^*) = P_N^*(r^*) + \frac{r^*}{2}\frac{dP_N^*(r^*)}{dr^*}. \quad (9)$$

While the *tanh* function fits the density and the normal pressure component very well, the triangle data points for P_T^* scatter considerably along the fitting curve (dashed line) due to the dependence on the first-order derivative in Eq. (9). Fluctuations of the data points for P_T^* are more severe in the droplet case as shown in Fig. 7(c) than that for other cases, since the counting statistics in the droplet center region becomes very poor due to the small volume of the shell for the averaging process.

For the pressure components of the thin film a recently developed method [18] has been applied and results in the distributions shown in Fig. 7(b). In this method the expressions are based on the Cartesian coordinates and given as

$$p_N^*(k) = \rho^*(k)T^* - \frac{1}{V_{sl}^*}\left\langle \sum_{i,j}^{k}\left(\frac{z_{ij}^{*2}}{r_{ij}^*}\Phi^{*\prime}(r_{ij}^*)f_{k,ij}\right)\right\rangle, \quad (10)$$

$$p_T^*(k) = \rho^*(k)T^* - \frac{1}{V_{sl}^*}\left\langle \sum_{i,j}^{k}\left(\frac{\frac{1}{2}(x_{ij}^{*2}+y_{ij}^{*2})}{r_{ij}^*}\Phi^{*\prime}(r_{ij}^*)f_{k,ij}\right)\right\rangle, \quad (11)$$

where $\rho^*(k)$ is the density in slab k instead of shell k used in the spherical coordinate, V_{sl} is the volume of the slab ($V_{sl} = L_x L_y L_{sl}$), L_{sl} is the slab thickness, and the term $f_{k,ij}$ is defined as the ratio of the length that the force F_{ij} covers in slab k to the total length of the force. Before this method is introduced, the pressure components have been calculated from Eqs. (10) and (11) with $f_{k,ij} = 1$, which generates false negative values of the normal component in the interfacial region for a planar interface. Details are explained in recent work [18].

The pressure variations differ from each other interfacial region, while the local density increases from vapor-phase to liquid-phase for all cases. For a bubble the normal pressure component decreases from vapor-phase to liquid-phase, for a droplet it increases, and for a thin film it remains constant as that of vapor-phase. This comparison supports the accurate prediction of pressure components using the modified method for thin films.

While surface tensions for a droplet can be estimated by the thermodynamic or the mechanical route [1], there has not been any discussion on the surface tension for a bubble. In this study, the mechanical route is employed to calculate the bubble surface tension. From the mechanical arguments for the force and torque and the mechanical stability conditions an expression for the surface tension of a spherical interface [1,2] can be derived as

$$\gamma_S^{*3} = -\frac{1}{8}\left(P_l^* - P_g^*\right)^2 \int_0^\infty r^{*3}\frac{dP_N^*}{dr^*}\,dr^* \quad (12)$$

and the radius of the surface of tension can be obtained from Eq. (7) as

$$R_S^* = \frac{2\gamma_S^*}{P_l^* - P_g^*}. \quad (13)$$

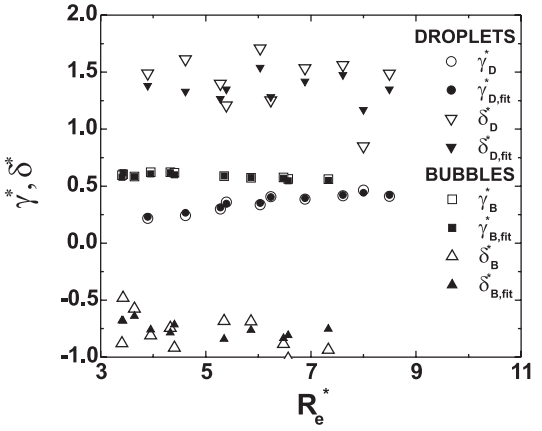

Fig. 8. Surface tension and Tolman's length for bubbles and droplets.

Fig. 8 compares surface tensions and Tolman's length introduced in Eqs. (1) and (2) for droplets and bubbles with respect to the equimolar dividing radius R_e^*, which can be given as

$$R_e^{*3} = \frac{1}{\rho_g^* - \rho_l^*}\int_0^\infty r^{*3}\frac{d\rho^*}{dr^*}\,dr^*. \quad (14)$$

Open symbols represent the data directly obtained from the MD simulation, and solid ones denote the data estimated from the fitting functions. Surface tensions from the raw data and the fitting functions agree well with each other, while Tolman's lengths directly obtained from simulation scatter more widely than those from fitting functions. In general, as R_e^* increases, surface tension for bubbles decreases very slightly, but that for droplets increases. Tolman's lengths for droplets scatter around a value of 1.3, but those for bubbles scatter around −0.7. It should be noted that the sign of Tolman's length is negative for bubbles, which implies that the surface tension of a bubble might be larger than that of a planar interface from Eq. (1). Here, the radii, R_e^* and R_S^*, are taken as positive to simplify the comparison.

Fig. 9 compares surface tensions from the simulation and from theoretical estimation by the simplified and the rigorous Tolman equations [13]. The simplified equation is given by Eq. (1) and the rigorous one is

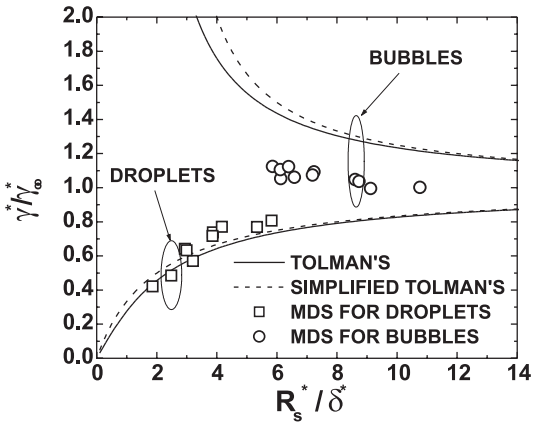

Fig. 9. Comparison of surface tensions from MD simulation and Tolman's theory for bubbles and droplets.

$$\ln\left(\frac{\gamma_S^*}{\gamma_\infty^*}\right) = \int_\infty^{r^*} \frac{(2\delta^*/r^{*2})\left(1+\delta^*/r^*+\frac{1}{3}\delta^{*2}/r^{*2}\right)}{1+(2\delta^*/r^{*2})\left(1+\delta^*/r^*+\frac{1}{3}\delta^{*2}/r^{*2}\right)}\,\mathrm{d}r^*. \quad (15)$$

The simplified equation agrees very well with the rigorous expression except for small radii. For droplets, surface tensions calculated from the MD simulation agree with the prediction from the Tolman equation. For bubbles, however, surface tensions from the simulations are smaller than those from the Tolman equation and larger than the value of the planar interface within a 15% range, even though there exists a decreasing tendency with the increase of bubble radii. Here, γ_∞^* is 0.545 in this case, which is obtained from the equation

$$\gamma_\infty^* = \frac{1}{2}\int_{-\infty}^{\infty}\left(P_N^* - P_T^*\right)\mathrm{d}z^*, \quad (16)$$

where P_N^* and P_T^* are calculated from Eqs. (10) and (11). First, the discrepancy between the simulation results and the theoretical predictions may come from the periodic boundary conditions used in the MD simulations in contrast to the infinite boundary condition for the theoretical estimation. Due to the periodicity of the simulation condition each bubble is exposed to the influence of adjacent bubbles and the liquid-phases between bubbles are confined within the calculation domain. Secondly, as the bubble size decreases, the liquid-phases are severely stretched to satisfy the Laplace equation and the shapes of bubbles are significantly distorted, while theories are based on a spherical shape. Thirdly, the density and pressure distributions are not spherically symmetric, since the liquid-phase region between the adjacent bubbles is not usually thick enough to maintain the spherical uniformity as discussed for Fig. 5. Lastly, the theoretical model is based on a stationary system, while the bubble shape varies considerably during the production period.

A simple binary molecule system of solvent molecules (A) and solute molecules (B) is simulated to investigate the effect of foreign molecules on surface tension of a bubble. These molecules interact with each other based on the Lennard–Jones potential,

$$\Phi^*(r_{ij}^*) = 4\left[\left(\frac{1}{r_{ij}^*}\right)^{12} - \alpha_{AB}\left(\frac{1}{r_{ij}^*}\right)^{6}\right], \quad (17)$$

where the parameter α_{AB} controls the miscibility of the solute and solvent molecules [12,19] and ε and σ are the same for all interactions. It is noted that the parameters for the same molecules α_{AA} and α_{BB} are unity. For α_{AB} less than unity the attractive force between A and B molecules is smaller than that between the same-type molecules and thus resulting in a low solubility (immiscibility) or phase separation. For α_{AB} greater than unity the affinity between A and B molecules is higher than that between the same-type molecules. In this case some solute molecules attract solvent molecules and may reorder the arrangement of the solvent molecules as in the solvation process.

In a previous paper [12] it was shown that even a small amount of solute molecules could expedite a bubble nucleation, although the dispersion of the foreign molecules into the solvent molecules varies significantly according to the value of the parameter α_{AB}. Fig. 10 describes the surface tension variation with respect to α_{AB}. For the concentration of foreign molecules $y_B = 0.5\%$ surface tension is not influenced much by the value of α_{AB}, since that of binary molecule systems ($\alpha_{AB} \neq 1$) is slightly smaller than that of the single-component molecule system ($\alpha_{AB} = 1$). For a higher concentration of the solute molecules ($y_B = 2\%$) the surface tension has a tendency to decrease as α_{AB} decreases for $\alpha_{AB} < 1$, but the maximum of the surface tension appears around $\alpha_{AB} = 1.5$, which necessitates the further research on the interfacial tension of a binary system.

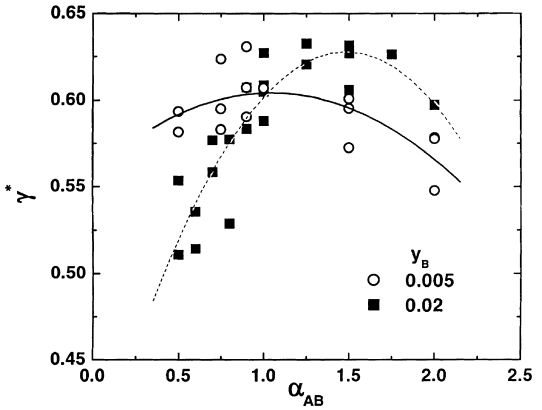

Fig. 10. Surface tensions of a binary molecule system for $\rho_{avg}^* = 0.66$ and $L^* = 15$.

4. Summary

This study employs the molecular dynamics simulation method to investigate the surface tension of small bubbles and their characteristics. To define a bubble, a void grid structure is constructed and the calculation domain is centered artificially on the mass center of void packets.

A smaller calculation domain yields a more stable field because the wavelength of fluctuation is limited by the calculation cell size. For this reason, the average density for stable bubble nucleation decreases as the domain size decreases down to a critical cell size. Below this cell size, the shape of the bubble is significantly distorted and bubbles in adjacent calculation domains tend to merge due to the break-up of the liquid-phase region between the domains.

Based on the mechanical route and the assumption of spherical bubble shape, the surface tension of a bubble is calculated from the density profile and from the normal and the transverse components of the pressure tensor. With the decrease of the bubble radius, surface tensions increase very slightly compared to the considerable decrease of droplet surface tensions as predicted by the Tolman equation.

For a binary system, the surface tension decreases slightly compared to that for a single-component system with a small addition of foreign molecules. For a larger concentration of foreign molecules the surface tension decreases significantly for affinity coefficients $\alpha_{AB} < 1$ and the maximum value appears at $\alpha_{AB} > 1$.

Acknowledgements

The authors gratefully acknowledge the financial support from the US Department of Energy and the National Science of Foundation. S.H. Park has been partially supported for this research by grant from the Korean Science and Engineering Foundation under Contract No. 1999-1-304-002-5.

References

[1] S.M. Thompson, K.E. Gubbins, J.P.R.B. Walton, R.A.R. Chantry, J.S. Rowlinson, A molecular dynamics study of liquid drops, J. Chem. Phys. 81 (1984) 530–542.

[2] J.S. Rowlinson, B. Widom, Molecular Theory of Capillarity, Oxford University Press, New York, 1982.

[3] J. Israelachvili, Intermolecular and Surface Forces, second ed., Academic Press, San Diego, 1992.

[4] J.G. Weng, S.H. Park, C.L. Tien, Interfacial ambiguities in microdroplets and microbubbles, Microscale Thermophys. Eng. 4 (2000) 83–87.

[5] M.P. Allen, D.J. Tildesley, Computer Simulation of Liquids, Oxford University Press, Oxford, 1987.

[6] J.M. Haile, Molecular Dynamics Simulation, Wiley, New York, 1992.

[7] S. Maruyama, Molecular dynamics method for microscale heat transfer, in: W.J. Minkowycz, E.M. Sparrow (Eds.), Advances in Numerical Heat Transfer, vol. 2, Taylor & Francis, 2000, pp. 189–226.

[8] W.J. Yang, K.T. Tsutsui, Overview of boiling on microstructures-macro bubbles from micro heaters, Microscale Thermophys. Eng. 4 (2000) 7–24.

[9] M.E. Parker, D.M. Heyes, Molecular dynamics simulation of stretched water: local structure and spectral signatures, J. Chem. Phys. 108 (1998) 9039–9049.

[10] T. Kinjo, M. Matsumoto, Cavitation processes and negative pressure, Fluid Phase Equilibria 144 (1998) 343–350.

[11] T. Kinjo, K. Ohguchi, K. Yasuoka, M. Matsumoto, Computer simulation of fluid phase change: vapor nucleation and bubble formation dynamics, Comput. Mater. Sci. 14 (1999) 138–141.

[12] S.H. Park, J.G. Weng, C.L. Tien, Cavitation and bubble nucleation using molecular dynamics simulation, Microscale Thermophys. Eng. 4 (2000) 161–175.

[13] R.C. Tolman, The effect of droplet size on surface tension, J. Chem. Phys. 17 (1949) 333–337.

[14] W.C. Swope, H.C. Anderson, P.H. Berens, K.R. Wilson, A computer simulation method for the calculation of equilibrium constants for the formation of physical clusters of molecules: application to small water clusters, J. Chem. Phys. 76 (1982) 637–649.

[15] S. Maruyama, T. Kimura, A molecular dynamics simulation of a bubble nucleation on solid surface, in: Proceedings of the Fifth ASME/JSME Joint Thermal Engineering Conference, San Diego, CA, 1999, pp. 1–7.

[16] N.B. Vargaftik, Tables on the Thermophysical Properties of Liquids and Gases, second ed., Hemisphere, Washington, DC, 1975, p. 543.

[17] D. Roylance, Mechanics of Materials, Wiley, New York, 1996, pp. 251–254.

[18] J.G. Weng, S.H. Park, J.R. Lukes, C.L. Tien, Molecular dynamics investigation of thickness effect on liquid films, Journal of Chemical Physics 113 (2000) 5917–5923.

[19] E. Diaz-Herrera, J. Alejandre, G. Ramirez-Santiago, F. Forstmann, Interfacial tension behavior of binary and ternary mixtures of partially miscible Lennard–Jones fluids: a molecular dynamics simulation, J. Chem. Phys. 110 (1999) 8084–8089.